# Plasma-Deposited Fluorocarbon Films: Insulation Material for Microelectrodes and Combined Atomic Force Microscopy–Scanning Electrochemical Microscopy Probes

**ARTICLE** *in* ANALYTICAL CHEMISTRY · AUGUST 2008

Impact Factor: 5.64 · DOI: 10.1021/ac800246q · Source: PubMed

*Anal. Chem.* **2008,** *80,* 5260–5265

# Plasma-Deposited Fluorocarbon Films: Insulation Material for Microelectrodes and Combined Atomic Force Microscopy−Scanning Electrochemical Microscopy Probes

**Justyna Wiedemair,[†] Balamurali Balu,[‡] Jong-Seok Moon,[†] Dennis W. Hess,[‡] Boris Mizaikoff,[†] and Christine Kranz*,[†]**

*School of Chemistry and Biochemistry, and School of Chemical and Biomolecular Engineering, Georgia Institute of Technology, Atlanta, Georgia 30332*

**Pinhole-free insulation of micro- and nanoelectrodes is the key to successful microelectrochemical experiments performed in vivo or in combination with scanning probe experiments. A novel insulation technique based on fluorocarbon insulation layers deposited from pentafluoroethane (PFE, $CF_3CHF_2$) plasmas is presented as a promising electrical insulation approach for microelectrodes and combined atomic force microscopy−scanning electrochemical microscopy (AFM−SECM) probes. The deposition allows reproducible and uniform coating, which is essential for many analytical applications of micro- and nanoelectrodes such as, e.g., in vivo experiments and SECM experiments. Disk-shaped microelectrodes and frame-shaped AFM tip-integrated electrodes have been fabricated by postinsulation focused ion beam (FIB) milling. The thin insulation layer for combined AFM−SECM probes renders this fabrication technique particularly useful for submicro insulation providing radius ratios of the outer insulation versus the disk electrode (RG values) suitable for SECM experiments. Characterization of PFE-insulated AFM−SECM probes will be presented along with combined AFM−SECM approach curves and imaging.**

Pinhole-free and uniform insulation is a critical requirement for electroanalytical experiments at the micro- and nanoscale, particularly if quantitative analysis of an analyte is desired. The most common technique to insulate microelectrodes is encapsulation in glass; this procedure has been summarized in several reviews.[1–4] However, encapsulation in glass is usually applied for sealing microsized metal wires. Many applications of microelectrodes, e.g., for in vivo measurements or for specialized electrochemical scanning probes, require different insulation techniques. As a result, a number of different insulation approaches for encapsulation of microwires or etched nanoelectrodes have been reported.[5–20] Early approaches were based on simple dipping of the microwire into molten apiezon wax[5,21] or varnish[22,23] as well as translating the wire through molten paraffin.[15] Among the insulation procedures using electrodeposition, formation of electrophoretic paint layers by an electrochemically induced pH shift is currently the most popular technique for submicrometer-sized electrodes. Both cathodic-[13,16,24–27] and anodic-based[12,13,18,28–30] electrophoretic paints have been used, and insulation is achieved during a postpolymerization curing process. During heat curing, a conically shaped electrode is usually exposed due to shrinking

* Corresponding author. E-mail: christine.kranz@chemistry.gatech.edu.
† School of Chemistry and Biochemistry.
‡ School of Chemical and Biomolecular Engineering.

(1) Fan, F. R. F.; Demaille, C. In *Scanning Electrochemical Microscopy*; Bard, A. J., Mirkin, M. V., Eds.; Marcel Dekker: New York, 2001; pp 75−110.
(2) Zoski, C. G. *Electroanalysis* **2002**, *14*, 1041–1051.
(3) Wightman, R. M.; Wipf, D. O. In *Electroanalytical. Chemistry*; Bard, A. J., Ed.; Marcel Dekker, Inc.: New York, 1989; Vol. 15, pp 267−353.
(4) Fleischmann, M.; Pons, S.; Rolison, D. R.; Schmidt, P. P. *Ultramicroelectrodes*; Datatech Systems Inc.: Morgantown, NC, 1987; pp 226−238.
(5) Nagahara, L. A.; Thundat, T.; Lindsay, S. M. *Rev. Sci. Instrum.* **1989**, *60*, 3128–3130.
(6) Loeb, G. E.; Peck, R. A.; Martyniuk, J. *J. Neurosci. Methods* **1995**, *63*, 175–183.
(7) Potje-Kamloth, K.; Janata, J.; Josowicz, M. *Ber. Bunsen-Ges. Phys. Chem.* **1989**, *93*, 1480–1485.
(8) Zhang, X. J.; Ogorevc, B. *Anal. Chem.* **1998**, *70*, 1646–1651.
(9) Koh, D.-S.; Hille, B. *J. Neurosci. Methods* **1999**, *88*, 83–91.
(10) Liu, B.; Rolland, J. P.; DeSimone, J. M.; Bard, A. J. *Anal. Chem.* **2005**, *77*, 3013–3017.
(11) El-Deen, E.; El-Giar, M.; Wipf, D. O. *Electroanalysis* **2006**, *18*, 2281–2289.
(12) Schulte, A.; Chow, R. H. *Anal. Chem.* **1996**, *68*, 3054–3058.
(13) Slevin, C. J.; Gray, N. J.; Macpherson, J. V.; Webb, M. A.; Unwin, P. R. *Electrochem. Commun.* **1999**, *1*, 282–288.
(14) Penner, R. M.; Heben, M. J.; Lewis, N. S. *Anal. Chem.* **1989**, *61*, 1630–1636.
(15) Zhang, B.; Wang, E. *Electrochim. Acta* **1994**, *39*, 103–106.
(16) Qiao, Y.; Chen, J.; Guo, X.; Cantrell, D.; Ruoff, R.; Troy, J. *Nanotechnology* **2005**, *16*, 1598–1602.
(17) Schwank, M.; Muller, U.; Hauert, R.; Rossi, R.; Volkert, M.; Wintermantel, E. *Sens. Actuators, B* **1999**, *B56*, 6–14.
(18) Bach, C. E.; Nichols, R. J.; Beckmann, W.; Meyer, H.; Schulte, A.; Besenhard, J. O.; Jannakoudakis, P. D. *J. Electrochem. Soc.* **1993**, *140*, 1281–1284.
(19) Strein, T. G.; Ewing, A. G. *Anal. Chem.* **1992**, *64*, 1368–1373.
(20) Lambie, B. A.; Orwar, O.; Weber, S. G. *Anal. Chem.* **2006**, *78*, 5165–5171.
(21) Mirkin, M. V.; Fan, F. R. F.; Bard, A. J. *J. Electroanal. Chem.* **1992**, *328*, 47–62.
(22) Vitus, C. M.; Chang, S. C.; Schardt, B. C.; Weaver, M. J. *J. Phys. Chem.* **1991**, *95*, 7559–7563.
(23) Gewirth, A. A.; Craston, D. H.; Bard, A. J. *J. Electroanal. Chem.* **1989**, *261*, 477–482.
(24) Gray, N. J.; Unwin, P. R. *Analyst (Cambridge, U.K.)* **2000**, *125*, 889–893.
(25) Chen, S.; Kucernak, A. *J. Phys. Chem. B* **2002**, *106*, 9396–9404.
(26) Abbou, J.; Demaille, C.; Druet, M.; Moiroux, J. *Anal. Chem.* **2002**, *74*, 6355–6363.
(27) Chen, S.; Kucernak, A. *Electrochem. Commun.* **2002**, *4*, 80–85.
(28) Macpherson, J. V.; Unwin, P. R. *Anal. Chem.* **2000**, *72*, 276–285.
(29) Conyers, J. L.; White, H. S. *Anal. Chem.* **2000**, *72*, 4441–4446.
(30) Lee, Y.; Bard, A. J. *Anal. Chem.* **2002**, *74*, 3626–3633.



10.1021/ac800246q CCC: $40.75 
Published on Web 05/30/2008

of the polymer from the apex of the wire. Insulation of carbon fiber electrodes has also been reported by electropolymerization of poly(phenylene oxide)[7,19] or by electrophoretic deposition of photoresist.[20] As an alternative to electropolymerization techniques, carbon fibers have been insulated with poly(tetrafluoroethylene)[8] by melting Teflon around a carbon fiber using a pipet puller. Similar materials were reported as a "Teflon-like liquid" based on photocurable highly fluorinated functionalized perfluoropolyether for insulation of metal and carbon microelectrodes.[10] Commercial microelectrodes insulated with Parylene C, a xylylene derivate, which is deposited by chemical vapor polymerization, are available.[6,31,32] Chemical vapor deposition (CVD) processes for thin-film silica deposition,[33] polyimide,[34] and plasma-enhanced CVD (PECVD) of perfluorooctane[35] for insulation have also been reported.

Recent developments in scanning probe technology resulted in the combination of atomic force microscopy (AFM) and scanning electrochemical microscopy (SECM).[28,36–43] This combination is based on a bifunctional scanning probe microscopy (SPM) tip with an electrode integrated into an AFM tip or by fabricating a nanoelectrode bent into the shape of an AFM cantilever. In both cases pinhole-free insulation is crucial for the successful combination of scanning probe experiments. Cantilever-shaped nanoelectrodes have been insulated with anodic and cathodic electrophoretic paint as described above. In the case of anodic paint insulation, conical nanoelectrodes were obtained due to paint shrinking during the curing process. Cantilever-shaped spherical gold electrodes were insulated with cathodic paint by scanning the potential between 0 and 5 V during paint deposition.[26] Up to 80% of the insulated electrodes revealed complete coverage, and exposure of the spherical electrode geometry was achieved by applying a high potential, thereby removing the insulation layer at the apex of the tip. In general, insulation techniques based on batch processes are preferred in order to ensure uniformity and reproducibility of the coating procedure.

Microfabricated bifunctional AFM−SECM probes described previously are mostly insulated with silicon nitride and/or silicon oxide deposited by PECVD. Alternatively, Parylene C has been applied to insulate combined AFM−SECM probes with recessed electrodes.[38,44] Within the present study, a novel insulation technique for combined AFM−SECM probes based on plasma-deposited fluorocarbon films using pentafluoroethane (PFE, $CF_3CHF_2$) as a precursor is reported.

Plasma polymerization is a widely applied technique for the fabrication of thin polymer films from a variety of organic precursors.[45–48] Excitation of the precursor in an electrical discharge leads to the deposition of a highly cross-linked film at an exposed substrate surface. The resulting films are typically mechanically and thermally stable, as well as chemically inert and insoluble, and have been used for a variety of applications due to these desirable properties.[49] The chemical structure and composition of plasma-deposited films can be modified by varying process conditions such as radio frequency (rf) power level, reactor pressure, substrate temperature, frequency of the discharge, selection of the monomer(s), and monomer(s) flow rate(s).[50] This tunable property of the plasma processing provides multiple degrees of freedom conducive to the optimization of deposited insulation layers.

Insulation layers presented in this study were deposited in a parallel plate rf (13.56 MHz) plasma reactor using PFE as a precursor gas.[51] Fluorocarbon films prepared from PFE vapors have previously been extensively studied with regard to their thermal stability,[52] the plasma chemistry involved in deposition,[53] and their electrical properties.[54] Favorable characteristics of fluorocarbon layers include their high resistivity, chemical inertness, biocompatibility, and conformal step coverage during thin-film deposition,[55] therefore providing an attractive choice for novel thin-film insulation strategies. Furthermore, for electrochemical SPM experiments, the relative thickness $rg/a$ (RG), where rg is the radius of the insulation and $a$ is the radius of the active electrode area, plays an important role.[56] Nanoelectrodes or combined AFM−SECM probes with small RG values are desirable for electrochemical scanning probe experiments. Indeed, using the proposed strategy, insulating films with a thickness <300 nm could be achieved. Besides small RG values, the thin insulation layer and fast milling rates for the deposited films also lead to a decrease in focused ion beam (FIB) milling time, thereby reducing the overall process time and cost for probe fabrication. In addition,


(31) Loeb, G. E.; Bak, M. J.; Salcman, M.; Schmidt, E. M. *IEEE Trans. Biomed. Eng.* **1977**, *24*, 121–128.
(32) Noordegraaf, J. *Med. Dev. Technol.* **1997**, *8*, 14–20.
(33) Abe, T.; Itaya, K.; Uchida, I. *Chem. Lett.* **1988**, 399–402.
(34) Lee, B.-J.; Kim, H.-G.; Lee, D.-C. *Surf. Coat. Technol.* **2002**, *150*, 182–187.
(35) Biloiu, C.; Biloiu, I. A.; Sakai, Y.; Sugawara, H.; Ohta, A. *J. Vac. Sci. Technol., A* **2004**, *22*, 1158–1165.
(36) Shin, H.; Hesketh, P. J.; Mizaikoff, B.; Kranz, C. *Anal. Chem.* **2007**, *79*, 4769–4777.
(37) Dobson, P. S.; Weaver, J. M. R.; Holder, M. N.; Unwin, P. R.; Macpherson, J. V. *Anal. Chem.* **2005**, *77*, 424–434.
(38) Kueng, A.; Kranz, C.; Mizaikoff, B.; Lugstein, A.; Bertagnolli, E. *Appl. Phys. Lett.* **2003**, *82*, 1592–1594.
(39) Macpherson, J. V.; Unwin, P. R. *Anal. Chem.* **2001**, *73*, 550–557.
(40) Kranz, C.; Friedbacher, G.; Mizaikoff, B.; Lugstein, A.; Smoliner, J.; Bertagnolli, E. *Anal. Chem.* **2001**, *73*, 2491–2500.
(41) Davoodi, A.; Pan, J.; Leygraf, C.; Norgren, S. *Electrochem. Solid-State Lett.* **2005**, *8*, B21–B24.
(42) Fasching, R. J.; Tao, Y.; Prinz, F. B. *Sens. Actuators, B* **2005**, *B108*, 964–972.
(43) Gullo, M. R.; Frederix, P. L. T. M.; Akiyama, T.; Engel, A.; de Rooij, N. F.; Staufer, U. *Anal. Chem.* **2006**, *78*, 5436–5442.
(44) Heintz, E. L. H.; Kranz, C.; Mizaikoff, B.; Noh, H.-S.; Hesketh, P.; Lugstein, A.; Bertagnolli, E. *Proceedings of the 2001 1st IEEE Conference on Nanotechnology*, NANO 2001 (Cat. No. 01EX516), Maui, HI, 2001; pp 346−351.
(45) Takahashi, Y.; Iijima, M.; Inagawa, K.; Itoh, A. *J. Vac. Sci. Technol., A* **1987**, *5*, 2253–2256.
(46) Kagami, Y.; Yamauchi, T.; Osada, Y.; Yoshizawa, I. *J. Appl. Phys.* **1990**, *68*, 610–616.
(47) Vaswani, S.; Koskinen, J.; Hess, D. W. *Surf. Coat. Technol.* **2005**, *195*, 121–129.
(48) Tamirisa, P. A.; Koskinen, J.; Hess, D. W. *Thin Solid Films* **2006**, *515*, 2618–2624.
(49) Shi, F. F. *Surf. Coat. Technol.* **1996**, *82*, 1–15.
(50) Biederman, H., Ed. *Plasma Polymer Films*; Imperial College Press: London, 2004.
(51) Dobbs, G. T.; Balu, B.; Young, C.; Kranz, C.; Hess, D. W.; Mizaikoff, B. *Anal. Chem.* **2007**, *79*, 9566–9571.
(52) Agraharam, S.; Hess, D. W.; Kohl, P. A.; Bidstrup Allen, S. A. *J. Electrochem. Soc.* **2000**, *147*, 2665–2670.
(53) Agraharam, S.; Hess, D. W.; Kohl, P. A.; Bidstrup Allen, S. A. *J. Vac. Sci. Technol., A* **1999**, *17*, 3265–3271.
(54) Agraharam, S.; Hess, D. W.; Kohl, P. A.; Bidstrup Allen, S. A. *J. Electrochem. Soc.* **2001**, *148*, F102–F107.
(55) Jansen, H. V.; Gardeniers, J. G. E.; Elders, J.; Tilmans, H. A. C.; Elwenspoek, M. *Sens. Actuators, A* **1994**, *41*, 136–140.
(56) Zoski, C. G.; Mirkin, M. V. *Anal. Chem.* **2002**, *74*, 1986–1992.

the insulation process described can be performed at batch level ensuring uniform and reproducible coating results. In this study, fluorocarbon-insulated AFM−SECM probes and microwires were fabricated and characterized. In addition, combined AFM−SECM experiments were conducted and SECM approach curves with these advanced probes were performed.

## EXPERIMENTAL SECTION

**AFM−SECM Probe and Microelectrode Preparation.** Triangular $Si_xN_y$ probes for AFM measurements (Veeco, Woodbury, NY) were used for fabricating bifunctional AFM−SECM probes. The reflecting gold layer and underlying chrome layer of the commercial AFM probes were removed with gold (GE-8110, Transene, Danvers, MA) and chrome etchant solutions (CR7-S, Cyantek, Fremont, CA), respectively. A 10 nm titanium adhesion layer and a 120 nm gold film, respectively, were sputtered onto the AFM probes using a mask that defined a conductive line-shaped pattern onto the glass chip. Prior to PFE deposition, the cantilevers and gold microwires were cleaned for 20 min in an ozone chamber (BioForce Nanosciences, Ames, IA). In addition to PFE-coated gold microwires, PFE-coated gold microelectrodes were prepared by sealing the microwires into glass capillaries with a small section protruding from the end of the capillary, which was then insulated with a PFE layer. Electroactive areas were exposed by FIB milling.

**Solutions and Materials.** Potassium ferrocyanide and potassium chloride were purchased from Sigma-Aldrich (St. Louis, MO). Aqueous ferrocyanide solutions were prepared at a concentration of 0.01 mol $L^{-1}$ in 0.5 mol $L^{-1}$ potassium chloride as supporting electrolyte. For the long-time studies at PFE-coated AFM−SECM probes, a 0.002 mol $L^{-1}$ ferrocenemethanol and 0.5 mol $L^{-1}$ potassium chloride solution was used. To dissolve ferrocenemethanol, 5% ethanol was added to the aqueous solution. All solutions were prepared using deionized water with a resistivity of 18.2 MΩ·cm at 25 °C provided by a water purification system (Millipore, Billerica, MA). Gold microwires with a diameter of 25 $\mu$m were obtained from Goodfellow (U.K.). The sample for testing the imaging performance of the combined AFM−SECM probes was a pattern generated by bitmap-assisted FIB milling at a gold-coated (approximately 100 nm) glass slide (VWR, West Chester, PA) with a titanium adhesion layer of approximately 10 nm.

**Plasma Reactor Reagents.** Pentafluoroethane monomer gas (N4 grade, 99.99%) was kindly donated by Dr. Mike Mocella from Dupont (Wilmington, DE). Nitrogen (ultrahigh purity, 99.999%) and oxygen (ultrapure carrier, 99.996%) were purchased from Airgas Inc. (Radnor, PA). Argon carrier gas (ultrahigh purity, 99.99%) was purchased from Air Products and Chemicals Inc. (Allentown, PA).

**Plasma Deposition of PFE Films.** A 6 in. parallel plate plasma reactor described previously[51] was used to deposit PFE films at ~112 °C and 1 Torr. The bottom electrode was grounded and heated to 112 °C using Omegalux CIR 2015 cartridge heaters (Omega Engineering Inc., Stamford, CT). A type K thermocouple controlled by a Syskon RKC temperature controller (RKC Instrument Inc., Southbend, IN) was used to monitor the temperature at the bottom electrode. The power to the top electrode of the reactor was provided by an HF-300 13.56 MHz, 120 W rf power supply (ENI Power Systems, Rochester, NY). To minimize reflected power in the plasma system, a matching network (Heathkit SA-2060A, Heath Company, Benton Harbor, MI) was connected between the top electrode and the power supply. The reactor pressure was controlled using a pressure gauge (Varian Inc., Lexington, MA) and an Alcatel 2063 C rotary vacuum pump (Alcatel, Annecy, France). In addition to the AFM−SECM probes and gold microwires samples, a blank Si wafer was used as a control substrate during each plasma deposition. After loading the samples, the reactor was evacuated to a pressure of approximately 20 mTorr and $O_2$ gas was introduced into the reactor at a flow rate of 75 standard $cm^3$/min. The pressure was controlled and stabilized at approximately 1 Torr, and the plasma was turned on for 1 min for reactor surface cleaning purposes. In the following, the reactor was subsequently evacuated to approximately 20 mTorr, and PFE monomer along with argon gas were introduced at flow rates of 20 and 75 standard $cm^3$/min, respectively. After the reactor reached a stable (steady-state) pressure (approximately 1 Torr), the rf generator was activated to initiate film deposition.

**Apparatus.** An AFM (model 5500, Agilent Technologies, Chandler, AZ) with a liquid cell was used for combined measurements. To reduce the effect of environmental vibration and noise, the AFM was located in a vibration isolation chamber (Agilent Technologies, Chandler, AZ). For the three-electrode setup in the AFM liquid cell, a freshly chlorided silver wire (Goodfellow, U.K.) served as a silver quasi-reference electrode (AgQRE), a platinum wire was used as the auxiliary electrode, and the microelectrode integrated into the AFM tip was serving as the working electrode. All AFM images were tilt-corrected using the PicoScan 5.3.3 software (Agilent Technologies, Chandler, AZ). Electrochemical measurements were performed using a CHI 832A (bi)potentiostat (CH Instruments Inc., Austin, TX) in a home-built Faraday cage. The output signal of the potentiostat was directly transferred to an AD channel of the AFM controller, thereby enabling simultaneous correlation of the electrochemical data and the topographical image. All scanning electron microscopy (SEM) imaging and FIB milling steps were performed using either a Quanta 200 3D or a Nova 200 NanoLab DualBeam (FIB/SEM) system (FEI Company, Hillsboro, OR).

**Electrochemical Experiments.** Cyclic voltammetry (CV) was used to characterize the PFE-insulated AFM−SECM probes and Au microelectrodes. Voltammograms were recorded at the microelectrodes in 0.01 mol $L^{-1}$ ferrocyanide/0.5 mol $L^{-1}$ KCl solution versus SCE (saturated calomel electrode) at 0.02−0.1 V/s in a scan range of 0−0.6 V. For the long-time study of PFE film stability, cyclic voltammograms were recorded in 0.002 mol $L^{-1}$ ferrocenemethanol/0.5 mol $L^{-1}$ KCl solution versus SCE at 0.02 V/s in a scan range of −0.05 to 0.45 V in increments of 1−1.5 h for a total time period of 6 h. AFM−SECM imaging/approach experiments were acquired in 0.01 mol $L^{-1}$ ferrocyanide/0.5 mol $L^{-1}$ KCl solution, and the tip-integrated electrode was biased at 0.6 V versus AgQRE. Imaging experiments were performed in AFM contact mode at a scan speed of 0.36 lines/s (image size: 25 × 25 $\mu m^2$). For simultaneously recorded deflection and electrochemical approach curves, the cantilever sensitivity was determined from deflection−distance curves at gold surfaces prior to recording approach curves.

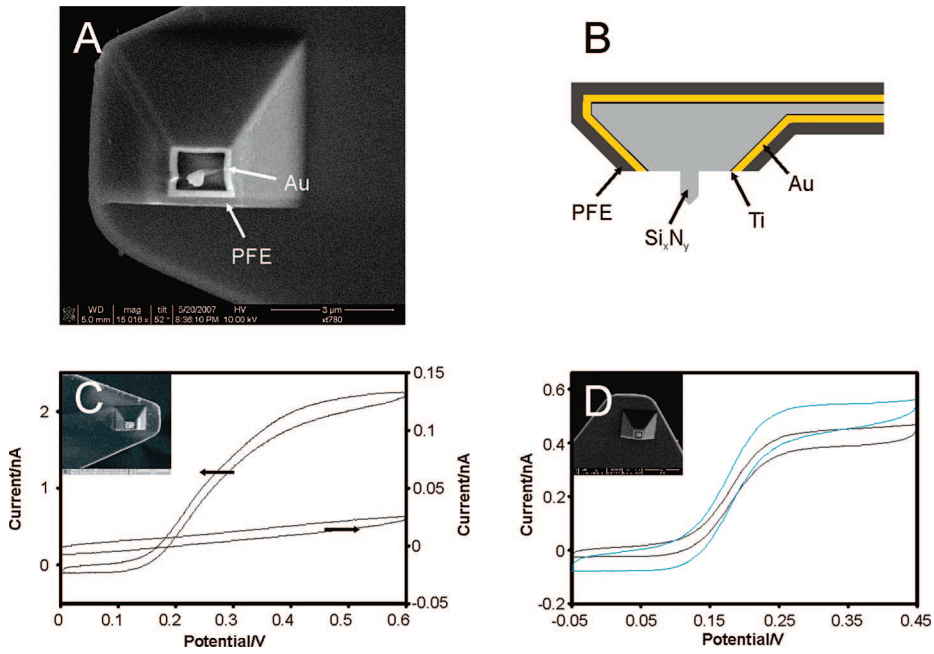


**Figure 1.** SEM image of a PFE-coated AFM−SECM cantilever after FIB milling (A); schematic cross section of the AFM−SECM probe illustrating the deposited layers (B); cyclic voltammograms of PFE-coated AFM−SECM probes before and after FIB milling (C) as well as before (black) and after (blue) the time study (D). The insets in (C) and (D) show SEM images of the AFM−SECM probes used in the particular electrochemical experiments. For the CVs in (C) an aqueous ferrocyanide solution at a concentration of 0.01 mol $L^{-1}$ in 0.5 mol $L^{-1}$ KCl was used; potentials were measured vs a SCE reference electrode, and CVs were recorded at 0.05 and 0.1 V/s. For the time study (D) a 0.002 mol $L^{-1}$ ferrocenemethanol solution in 0.5 mol $L^{-1}$ KCl was used, and the CVs were recorded at 0.02 V/s vs SCE. Frame edge lengths of the AFM tip-integrated electrodes were ~1.28 $\mu$m (C) and ~1.4 $\mu$m (D).

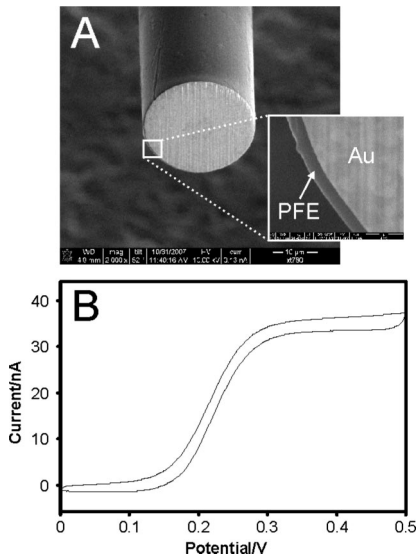


**Figure 2.** SEM image of a gold microwire after exposure of the electroactive area by FIB milling (A); cyclic voltammogram of a gold microelectrode after exposure of the electroactive area by FIB milling (B). The inset in (A) shows a high-magnification SEM image of the interface between PFE and gold. For the electrochemical experiment (B) the CV was recorded vs SCE in aqueous ferrocyanide solution at a concentration of 0.01 mol $L^{-1}$ in 0.5 mol $L^{-1}$ KCl; scan speed: 0.02 V/s.

## RESULTS AND DISCUSSION

**Plasma-Enhanced Deposition.** Figure 1A and Figure 2A show SEM images obtained from PFE-coated AFM−SECM probes and gold microwires after exposure of the electroactive area by FIB milling. The probe shown in Figure 1A has a PFE layer thickness of approximately 300 nm. In Figure 2A, a cross section of a gold microwire coated with approximately 400 nm of PFE is depicted. The inset shows a high-resolution SEM image, which demonstrates that very smooth cross sections of the electrode surfaces can be obtained without affecting the film. Furthermore, single crystallites in the polycrystalline gold microwire are clearly visible. The difference in thickness between samples of different shapes and materials is attributed to the following parameters: (i) a temperature gradient due to the sample (tip or wire) distance from the heated electrode and (ii) orientation of the exposed surface with respect to the ion bombardment direction and curvatures of the substrate inducing concentration gradients of the neutral species in diffusion-controlled plasma processes.

**Electrochemical Characterization.** After modification of the PFE-coated probes and exposure of the tip-integrated electrode by FIB milling, cyclic voltammograms were recorded to characterize the AFM−SECM probes prior to imaging. In addition, CVs were used to evaluate the long-term stability of the PFE layer in ferrocenemethanol solution.

The diffusion-limited steady-state current measured at microelectrodes is frequently used to evaluate the size of the electroactive area. Valuable information on the quality of the insulation layer can also be obtained from the shape of the CV. Figure 1C shows cyclic voltammograms recorded at a tip-integrated AFM−SECM probe in an aqueous ferrocyanide solution (0.01 mol $L^{-1}$ ferrocyanide in 0.5 mol $L^{-1}$ KCl) before and after FIB milling. The inset in Figure 1C shows an SEM image of the probe used during these experiments. The PFE layer reveals excellent insulating properties prior to the exposure of the tip-integrated electrode via FIB milling. Since no equation describing the steady-state current at frame electrodes is available, the equation for the

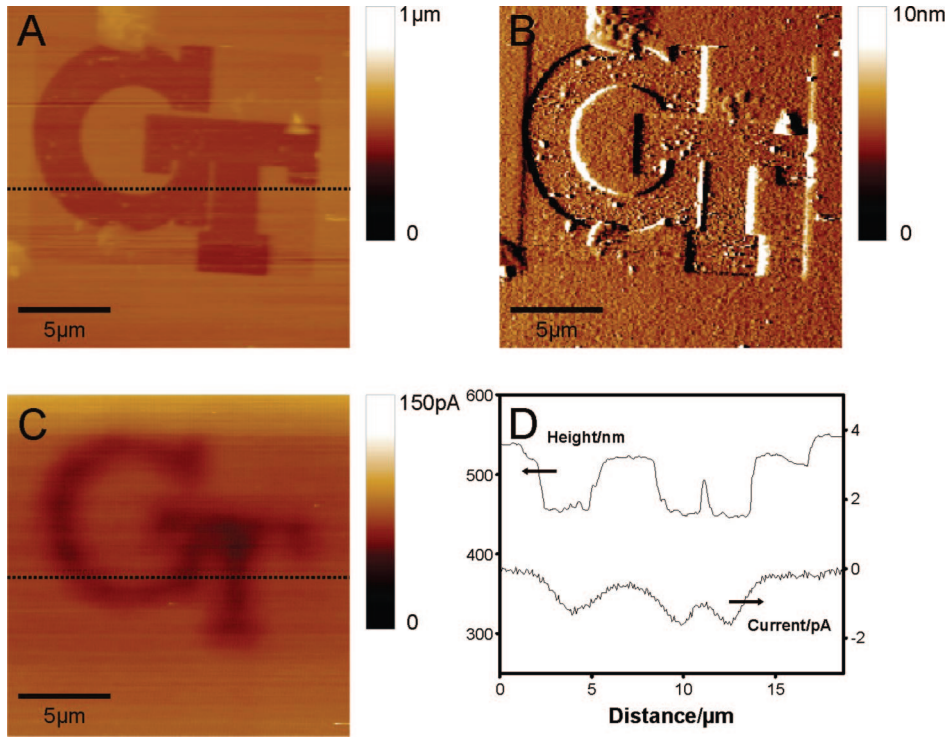


**Figure 3.** Simultaneously recorded AFM−SECM images at a FIB-patterned substrate. Images of the topography (A), deflection (B), and current (C) are shown. The dotted line in (A) and (C) represents the position of the cross section chosen for (D). The tip-integrated electrode was biased at 0.6 V (vs AgQRE) to oxidize ferrocyanide (0.01 mol $L^{-1}$ in 0.5 mol $L^{-1}$ KCl). The tip was scanned in AFM contact mode at a rate of 0.36 lines/s (original scan size: 25 × 25 $\mu m^2$). The edge length of the tip-integrated electrode frame was ~1.6 $\mu$m, and the tip height was ~0.54 $\mu$m.

steady-state current at a ring electrode, which is readily available from the literature, was used to obtain an estimate of the current response at the tip-integrated frame electrode. With the use of the dimensions determined from SEM images (frame edge length ~1.28 $\mu$m, frame thickness ~0.15 $\mu$m) and equations previously described[40,57,58] approximately 1.5 nA was obtained as theoretical value (0.01 mol $L^{-1}$ ferrocyanide, $D = 6.7 \times 10^{-6}$ $cm^2$ $s^{-1}$). Although there is a deviation of the measured value (approximately 2.3 nA) to the theoretical value, this discrepancy may be attributed to the fact that the geometry assumed is different from the actual geometry.

To evaluate the long-term stability of the PFE insulation layers in solution, studies over extended exposure periods were performed at tip-integrated frame electrodes. The AFM−SECM probe used within these studies was milled without reshaping an actual AFM tip during FIB fabrication. This probe is shown in the SEM image included in Figure 1D (inset). The probe was soaked in ferrocenemethanol, and cyclic voltammograms were recorded in increments of 1−1.5 h over a total time period of 6 h. Figure 1D shows CVs obtained before starting the time study (black curve) as well as after 6 h had elapsed (blue curve). The current increases by approximately 20%; however, the overall shape of the CV remains unaltered. Given that a typical AFM−SECM experiment takes about 2−3 h, the long-term stability of the probes is sufficient for such experiments, indicating that PFE layers are an attractive approach for insulating AFM tip-integrated electrodes.

To demonstrate the versatility of this novel insulation method, PFE-coated gold microwires and microelectrodes were prepared. The cross section of the wires was exposed using FIB milling. Figure 2B shows a cyclic voltammogram obtained at such a PFE-coated microelectrode in ferrocyanide solution (0.01 mol $L^{-1}$ ferrocyanide/0.5 mol $L^{-1}$ KCl).

**Combined Imaging.** PFE-coated AFM−SECM cantilevers were tested for their performance during simultaneous AFM−SECM imaging. The sample used for combined AFM−SECM experiments was patterned by FIB milling. An approximately 100 nm gold layer was deposited onto a glass slide with a titanium adhesion layer of approximately 10 nm. The pattern used for FIB milling was the logo of the Georgia Institute of Technology (GT) created as a bitmap and then uploaded to the FEI software. The gold was removed by milling, thereby exposing insulating glass at the letters of the logo. The AFM−SECM tip used for combined measurements had an edge length of ~1.6 $\mu$m and a tip length of ~0.54 $\mu$m.

The tip was biased at 0.6 V versus AgQRE in a solution of 0.01 mol $L^{-1}$ ferrocyanide and 0.5 M KCl as supporting electrolyte and scanned across the surface of the FIB-milled pattern. The steady-state current resulting from the oxidation of ferrocyanide was monitored at the tip-integrated electrode. As shown in Figure 3, the SECM feedback experiment revealed the expected behavior. Positive feedback was observed in the vicinity of the conducting gold surface, whereas the recessed insulating glass surface showed a negative feedback effect. Positive feedback results in an increased current recorded at the tip-integrated electrode due to the reduction (recycling) of Fe(III) at the conducting gold surface. Correspondingly, a decreased current, or also called negative feedback, is observed at the insulator due to hindered diffusion of ferrocyanide species to the tip-integrated electrode.

(57) Smythe, W. R. *J. Appl. Phys.* **1951**, *22*, 1499–1501.
(58) Szabo, A. *J. Phys. Chem.* **1987**, *91*, 3108–3111.

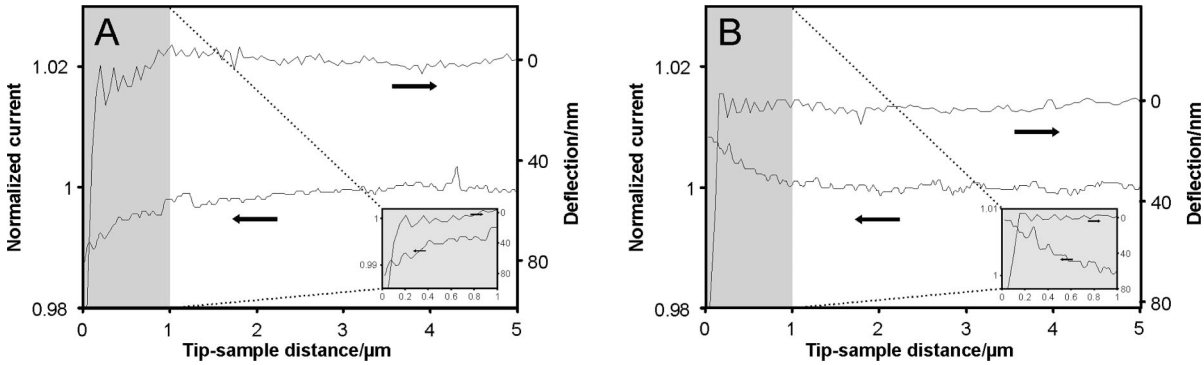


**Figure 4.** Simultaneously recorded approach and cantilever deflection curves measured with a PFE-coated bifunctional AFM−SECM tip showing negative feedback (A) at the glass surface and positive feedback (B) at the gold surface. The insets in (A) and (B) are magnified views of the curves close to the sample surface. The tip was biased at 0.6 V (vs AgQRE) in 0.01 mol $L^{-1}$ ferrocyanide and 0.5 mol $L^{-1}$ KCl. The edge length of the tip-integrated electrode frame was ~1.6 $\mu$m, and the tip height was ~0.54 $\mu$m.

Conducting and insulating current features are in excellent agreement with the simultaneously recorded topography image. The height profile depicted in Figure 3D demonstrates the electrochemical resolution obtained throughout the experiment. The thin strip of gold (approximately 400 nm wide) between the letters "G" and "T" of the Georgia Institute of Technology logo is clearly evident in the corresponding current image as an elevated current feature.

Combined AFM−SECM experiments using tip-integrated electrodes recessed from the apex of the tip offer the unique advantage of deconvoluting the electrochemical and topographical signal due to a constant tip−sample distance. During conventional constant height SECM experiments, topographical features may result in a current change, which cannot be exclusively attributed to a change in electrochemical activity due to the altered electrode−sample distance. As noted in Figure 3A (and part D), FIB milling of the GT bitmap resulted in a slight rectangular recess around the logo and the gold surface was slightly milled in the area surrounding the two letters. Although a step can be observed in the cross section of the height (Figure 3D), the corresponding area in the cross section of the current image does not show any evident change, thereby confirming the deconvolution of current and topography.

**Approach Curves.** PFE-coated bifunctional AFM−SECM probes were also used to record approach curves at insulating and conducting surface features.

Figure 4A and 4B shows representative normalized current (diffusion-limited steady-state current normalized by current measured in bulk solution) plots along with simultaneously recorded cantilever deflection curves recorded while approaching the substrate surface. In a standard "top-down" AFM configuration (where the tip is being scanned) the AFM stage approaches the tip in discrete steps (step size: 400 nm) in order to engage the tip at the surface. After each step, the piezo-scanner, which holds the AFM cantilever, is moved in the *z*-direction to detect the distance to the surface. If the cantilever is deflected, the stage stops approaching; otherwise approaching to the surface continues. Due to the short periodicity of moving/stopping steps, the *x*-scale (tip−sample distance) depicted in Figure 4A and 4B is an approximation derived from a time−signal curve and the total traveled distance. To convert cantilever deflection values from voltage (V) into a distance (nm), the sensitivity of the cantilever for the selected laser spot position was measured by recording deflection−distance curves at the Au substrate directly prior to the measurement of approach curves. Consequently, the slope of the force curve in the contact region can be used for calibration of the cantilever sensitivity.

As evident in Figure 4, the normalized current recorded at the AFM−SECM probe shows the typical behavior expected from SECM theory, if a microelectrode approaches an insulating (A) or conducting (B) surface. Insulators lead to a partial blocking of the redox mediator diffusion, thereby resulting in a current decrease, whereas a current increase can be observed at conductors due to recycling of the redox species at the substrate. Furthermore, it can be clearly seen in Figure 4 that the cantilever deflects rapidly after touching the surface, which coincides with the current decrease/increase.

## CONCLUSIONS

Pinhole-free insulation is a key element for electroanalytical measurements at the micro/nanoscale. This study introduces plasma-deposited PFE films as novel, uniform, and thin insulation materials for bifunctional AFM−SECM probes and microelectrodes. Successful electrochemical characterization of AFM tip-integrated electrodes insulated with PFE layers was performed. PFE-insulated microelectrodes were also fabricated thereby documenting the broad applicability of this new technology. Combined topographical and electrochemical measurements were obtained with bifunctional AFM probes at a FIB-patterned gold−glass substrate, revealing excellent electrochemical resolution. For confirming the applicability of PFE-coated probes, SECM approach curves were measured demonstrating positive and negative feedback effects depending on surface sample properties.

## ACKNOWLEDGMENT

J.W., J.-S.M., B.M., and C.K. acknowledge financial support by NIH Grant R01 EB000508. B.B. and D.W.H. thank Dr. Mike Mocella (Dupont) for donating the PFE monomer gas. The staff at MIRC (Georgia Institute of Technology) and the FIB$^2$ Center (Georgia Institute of Technology) is acknowledged for technical assistance.

Received for review February 4, 2008. Accepted April 25, 2008.

AC800246Q